

# La<sub>3</sub>Cu<sub>2</sub>VO<sub>9</sub>: A surprising variation on the YAlO<sub>3</sub> structure-type with 2D copper clusters of embedded triangles

Douglas A. Vander Griend<sup>a</sup>, Sylvie Malo<sup>a</sup>, Scott J. Barry<sup>a</sup>, Noura M. Dabbousch<sup>a</sup>, Kenneth R. Poeppelmeier<sup>a,\*</sup>, Vinayak P. Dravid<sup>b</sup>

<sup>a</sup> Department of Chemistry, Northwestern University, 2145 Sheridan Road, Evanston, IL 60208-3113, USA

<sup>b</sup> Department of Materials Science and Engineering, Northwestern University, 2137 Sheridan Road, Evanston, IL 60208-3108, USA

Received 5 July 2000; accepted 1 March 2001

## Abstract

La<sub>3</sub>Cu<sub>2</sub>VO<sub>9</sub> crystallizes in a heretofore unknown superstructural variation of the rare-earth hexagonal structure ( $P6_3/mmc$ ) for ABO<sub>3</sub> stoichiometries as characterized by X-ray, neutron and electron diffraction. The alternating hexagonal layers of LaO<sub>6/3</sub> and (Cu/V)O<sub>3/3</sub> resemble those of YAlO<sub>3</sub>, except that the copper and vanadium order to create an  $a\sqrt{13} \times a\sqrt{13} \times c$  supercell with  $P6_3/m$  symmetry. The B-cation coordination environments accommodate copper and vanadium in a two to one molar ratio. The Cu<sup>II</sup> lattice consists of nine atom clusters of triangles in triangles similar to a kagomé lattice. The phase is paramagnetic from 5 to 370 K with three temperature regimes that correspond closely to 1/9, 4/9, and 9/9 spins per copper. © 2001 Éditions scientifiques et médicales Elsevier SAS. All rights reserved.

**Keywords:** La<sub>3</sub>Cu<sub>2</sub>VO<sub>9</sub>; Kagomé; Copper clusters; Hexagonal structure

## 1. Introduction

The ABO<sub>3</sub> trivalent structural phase diagram has been intensely studied [1]. To a first approximation, the relationship between structure and ions can be classified geometrically, allowing structures to be predicted based on ionic radii [2]. In particular, the perovskite structure accommodates large A-cations that can form close packed AO<sub>3</sub> layers while ilmenite accommodates both the A- and B-cations in octahedral interstices. A growing number of compounds can be found at the interface between these two structures. If the A-cations are too small to form AO<sub>3</sub> layers, but too large to fill octahedral sites between close packed oxygen layers, then the rare-earth hexagonal structure can be the most thermodynamically stable [1]. YAlO<sub>3</sub> is a prime example [3]. Other examples include lanthanide aluminates (LnAlO<sub>3</sub>, Ln = Eu–Er) [3]

and indates (LnInO<sub>3</sub>, Ln = Eu, Gd and Dy) [4]. The fundamental unit cell ( $P6_3/mmc$ ,  $a \approx 4 \text{ \AA}$  and  $c \approx 11 \text{ \AA}$ ) consists of two ABO<sub>3</sub> units ( $Z = 2$ ). Both the A- and B-cations occupy separate hexagonal arrays as AO<sub>6/3</sub> layers of edge-sharing octahedra alternate with BO<sub>3/3</sub> layers (see Fig. 1). The coordination of the A-cations includes six oxygen in an octahedron with two more capping oxygen from the BO<sub>3/3</sub> plane. The size of the A-cation is crucial, and the aforementioned examples suggest that lanthanides from europium ( $r_{IX} = 112.0 \text{ pm}$ ) to erbium ( $r_{IX} = 106.2 \text{ pm}$ ) can facilitate this structure. However, the role of the B-cation in stabilizing the structure cannot be ignored. The ideal rare-earth hexagonal structure accommodates B-cations in trigonal bipyramidal sites ( $D_{3h}$ ).

Several homeotypic phases with multiple B-cations have been discovered recently. Ln<sub>4</sub>Cu<sub>3</sub>MoO<sub>12</sub> crystallizes in the rare-earth hexagonal structure for Ln = La, Pr, Nd and Sm–Tm [5]. In the lanthanum analogue, the Mo<sup>VI</sup>

\* Correspondence and reprints.

E-mail address: krp@northwestern.edu (K.R. Poeppelmeier).

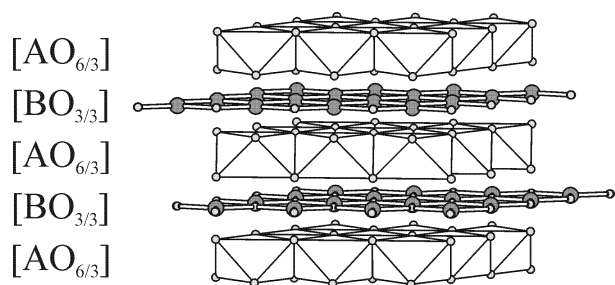


Fig. 1.  $ABO_3$  rare-earth hexagonal structure type:  $AO_{6/3}$  layers of edge-shared octahedra alternate with  $BO_{3/3}$  layers.

arrange in rectangles to yield a pseudo-monoclinic supercell ( $\beta \approx 90^\circ$ ) [6]. The coordination environments of both the  $Cu^{II}$  and the  $Mo^{VI}$  remain approximately trigonal as the in-plane oxygen simply shifts toward the  $Mo^{VI}$  and away from the  $Cu^{II}$  in order to preserve bond valence. The  $Cu^{II}$  atoms form trigonal clusters similar to a kagomé lattice. Geometric frustration creates the equivalent of two superimposable paramagnetic lattices that order antiferromagnetically at 5 and 400 K [7].  $Ln_2CuTiO_6$ ,  $Ln = Tb-Lu$ , is another family of cuprates which crystallize in the rare-earth hexagonal structure, but less is known about these phases [8]. Obviously, copper makes up only 50% of the transition metal proportion and the range of A-cations that can be incorporated at ambient pressure is restricted to lanthanides smaller than gadolinium.

Both families can be conceived as members of the homologous series:  $Ln_nCu_{n-1}M^{n+2}O_{3n}$ . The titanium and molybdenum families represent the  $n = 2$  and  $n = 4$  members, respectively. The relative amount of copper increases with  $n$  as does the feasible range of lanthanide cation size. Jansson et al. [9] have reported  $La_3Cu_2VO_9$  with a hexagonal unit cell of  $a = 14.4427(7)$  and  $c = 10.685(1)$  Å based on electron and powder X-ray diffraction, but the symmetry and structure of the phase were not reported. The similarity between the PXD pattern for  $La_3Cu_2VO_9$  and those for both  $La_2CuTiO_6$  and  $La_4Cu_3MoO_{12}$  is unmistakable. If the structure of the vanadate is based on the rare-earth hexagonal structure then it would be an  $n = 3$  member of the aforementioned series. The copper lattice could then be a partially substituted hexagonal lattice with potential for geometrically frustrated antiferromagnetism. The  $a$  parameter is  $\sqrt{13}$  times larger than that of the fundamental hexagonal unit cell, and this suggests yet a new class of superstructural modification for the  $YAlO_3$  structure type. We have ascertained the structure via X-ray, neutron and electron

diffraction experiments, and measured the magnetic susceptibility to corroborate the magnetic lattice.

## 2. Experimental

### 2.1. Synthesis

Polycrystalline  $La_3Cu_2VO_9$  was synthesized by solid state reactions in air. Stoichiometric amounts of lanthanum, copper, and vanadium oxide powders were thoroughly ground in an agate mortar, pressed into pellets, fired at  $1010^\circ C$  for 4 days with two intermittent grindings, and finally cooled at  $0.5^\circ C \text{ min}^{-1}$ . The sample was weighed before and after reaction.  $VO_2$  was used as the vanadium source and the 0.6% weight increase is consistent with the oxidation of  $V^{IV}$  to  $V^V$ .

### 2.2. X-ray diffraction

Powder X-ray diffraction (PX) data was recorded on a SCINTAG XDS 2000 diffractometer with Ni-filtered  $Cu-K_\alpha$  radiation. The data were collected in the  $2\theta$  range of  $5^\circ$  to  $120^\circ$  by scanning every  $0.015^\circ$  for 7.5 s.

### 2.3. Transmission electron microscopy

The sample was prepared by crushing a small piece in alcohol. The crystallites were deposited on a holey carbon film supported on a nylon grid. The electron diffraction (ED) was carried out on an 8100 Hitachi at 200 kV. A Hitachi HF2000 transmission electron microscope with cooled field emission gun was used to perform spectroscopy measurements. The cationic composition of the sample was verified by energy dispersive X-ray spectroscopy (EDS). The electron energy loss spectroscopy (EELS) was performed at 200 kV with a Gatan 666 parallel spectrometer.

### 2.4. Neutron powder diffraction (NPD)

The Intense Pulsed Neutron Source and Special Environment Powder Diffractometer at Argonne National Laboratory were used to collect time-of-flight data. Approximately 0.6 g of the sample was encapsulated in a thin-walled vanadium can, and data were collected for one hour at ambient temperature and pressure. Data from the detector banks at  $144.85^\circ 2\theta$  and at  $90.00^\circ 2\theta$  were used in the final Rietveld refinement. Reflections between 0.552 and 4.119 Å were used in the refinement. The

coherent scattering lengths for La, Cu, V and O were taken to be 8.24, 7.718,  $-0.3824$ , and  $5.805$  fm, respectively [10]. Rietveld refinement of the neutron data was carried out using the General Structure Analysis System (GSAS) [11].

Rietveld refinement of the X-ray data was used to determine the vanadium position since it is virtually transparent to neutron radiation. The atomic positions of the copper, lanthanum and oxygen from the neutron refinement were not changed and the thermal parameters ( $B_{\text{iso}}$ ) of the vanadium cations were set to  $0.64 \text{ \AA}^2$ .

### 2.5. Magnetic susceptibility

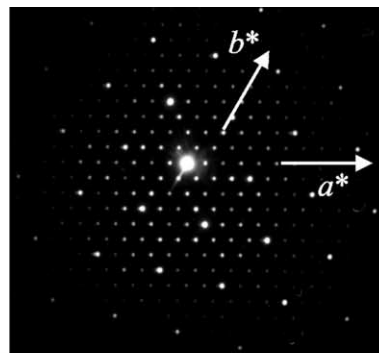
Zero-Field-Cooled (ZFC) susceptibility measurements were performed using a Quantum Design MPMS SQUID magnetometer from 5 to 370 K in an external field of 1000 Oe.

## 3. Results

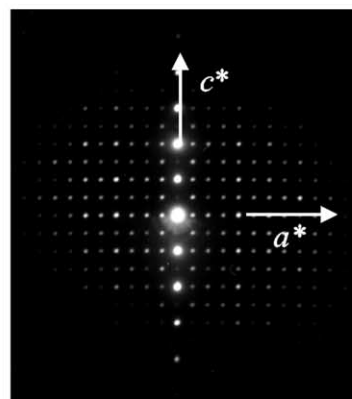
No impurity phases in the  $\text{La}_3\text{Cu}_2\text{VO}_9$  sample were detected in X-ray, neutron or electron diffraction experiments, and no substantial cation mass was lost during synthesis. EDS analysis performed on numerous crystals established cationic ratios of Cu:V of  $1.99(9)$  and La:V of  $2.9(2)$ , and the EELS spectra recorded on several crystals at the vanadium  $L_3/L_2$  edge indicated that the vanadium is in the  $+5$  oxidation state based on the  $L_3/L_2$  intensity ratio. This confirms the nominal phase stoichiometry of  $\text{La}_3\text{Cu}_2\text{VO}_9$  reported by Jansson et al. [9].

ED patterns show a set of intense reflections characteristic of the hexagonal subcell ( $a \approx 4 \text{ \AA}$  and  $c \approx 11 \text{ \AA}$ ), classically observed for the rare-earth hexagonal  $\text{YAIO}_3$  structure type. However, as previously reported, additional diffraction spots were observed which generate a new hexagonal lattice characterized by  $a \approx 14.4 = 4.0\sqrt{13} \text{ \AA}$  and  $c \approx 10.7 \text{ \AA}$  [9]. Large angle tilt electron diffraction (LATED) patterns along  $[0001]$ ,  $[1\bar{2}10]$  and  $[1\bar{1}00]$  evidence the only condition:  $000l: l = 2n$  (see Fig. 2).  $P6_3$ ,  $P6_3/m$  and  $P6_322$  are the three hexagonal space groups that have this condition alone. The convergent beam electron diffraction (CBED) pattern taken along  $[1\bar{1}00]$  (see Fig. 3) exhibits a mirror plane perpendicular to the  $c$ -axis indicating that the correct space group is  $P6_3/m$  (No. 176).

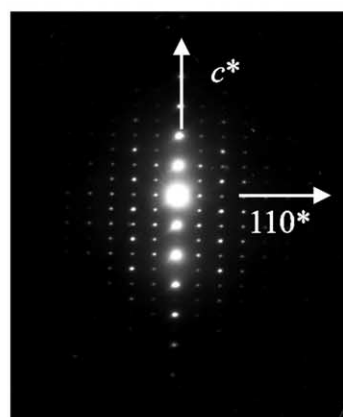
The unit cell seen in ED is thirteen times larger than the expected conventional hexagonal cell ( $a \approx 4 \text{ \AA}$ ,  $c \approx 11 \text{ \AA}$ ). The  $c$  parameter is the same as that for



a) LATED pattern along the  $[0001]$  zone axis



b) LATED pattern along the  $[1\bar{2}10]$  zone axis



c) LATED pattern along the  $[1\bar{1}00]$  zone axis

Fig. 2. LATED patterns of  $\text{La}_3\text{Cu}_2\text{VO}_9$  oriented (a)  $[0001]$ , (b)  $[1\bar{2}10]$  and (c)  $[1\bar{1}00]$  zone axes.

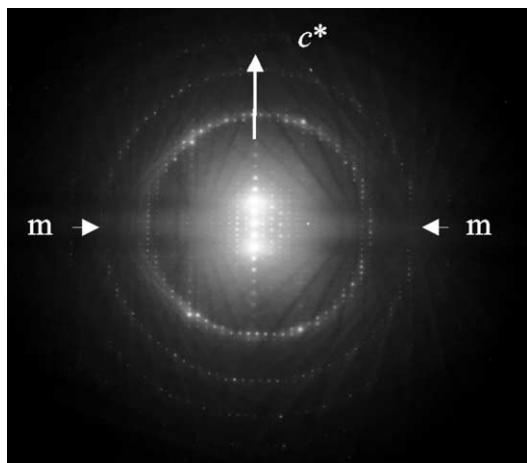


Fig. 3.  $[1\bar{1}00]$  CBED pattern of  $\text{La}_3\text{Cu}_2\text{VO}_9$  showing the mirror plane perpendicular to the  $c$ -axis and three higher order Laue zones.

the subcell, which implies that the hexagonal planes stack along  $c$  similarly, i.e. alternating  $\text{AO}_{6/3}$  and  $\text{BO}_{3/3}$  layers with a screw axis. This supercell is one of many hexagonal supercells that can exist in a hexagonal array because two lattice points can be exactly  $\sqrt{13}$  units apart. Relative distances of size  $\sqrt{3}$ ,  $\sqrt{7}$ , and  $\sqrt{21}$  are also possible. The relative area of any such hexagonal supercell equals  $n^2 + nm + m^2$ , where  $n$  and  $m$  are some natural numbers. The corresponding angle  $\chi$  between the unit vector and the supercell vector can be calculated as well:

$$\sin^2\left(\frac{\chi}{2}\right) = \frac{3m^2}{4(n^2 + nm + m^2)}.$$

Fig. 4 depicts how a thirteen times larger supercell ( $m = 1$  and  $n = 3$ ) relates to the fundamental cell ( $m = 0$  and  $n = 1$ ) common to the rare earth hexagonal phases.

There are at least two ways that such a cell could be realized. Both the A- and B-cation arrays in the  $\text{YAlO}_3$  structure type are hexagonal. A  $27.8^\circ$  rotation of the  $\text{AO}_{6/3}$  layers with respect to the  $\text{BO}_{3/3}$  layer would create an exact  $a\sqrt{13} \times a\sqrt{13} \times c$  supercell, and generate  $P6_3/m$  symmetry if the original subcell has  $P6_3/mmc$  symmetry. In this case, the B-cations are no longer positioned directly above and below the oxygen from the  $\text{AO}_{6/3}$  layer and the B-cation coordination environments are highly irregular. No rotational configuration has ever before been documented for this structure type, but has been seen in a zeolite system [12,13].

A second possibility would require the copper and vanadium to order in such a supercell. Initially this seems illogical because thirteen is a prime number, having no

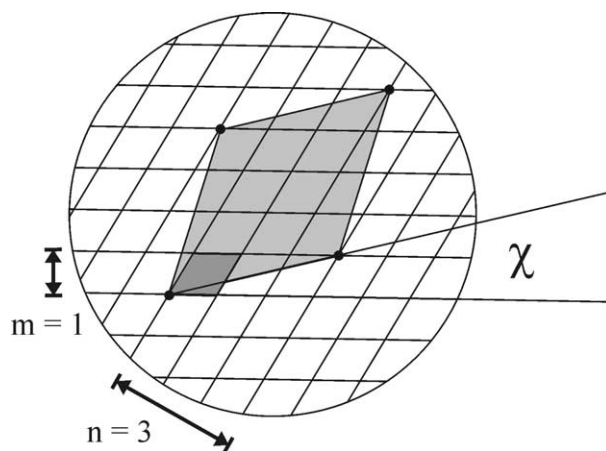


Fig. 4. The relationship between a simple hexagonal unit cell ( $n = 1$ ,  $m = 0$ ) and one exactly thirteen times larger ( $n = 3$ ,  $m = 1$ ).  $n$  and  $m$  are hexagonal vectors,  $\chi = 27.8^\circ$ .

factors other than itself and one. If the B-cations were to order, then a three times larger supercell would seem most appropriate.

Both the rotated and unrotated models were tested by refinement of neutron diffraction data. The initial atomic positions for the rotated one were deduced by rotation of the  $\text{AlO}_{3/3}$  positions in  $\text{YAlO}_3$  [3]. At first, vanadium and copper cations were distributed statistically on all B-cation sites, and the ratio of Cu to V was fixed at two. However, in the later stages of the refinement, vanadium, which is nearly transparent to the neutron radiation, could be assigned to two sites, V(1) and V(5). With this ordering, the positions of the  $\text{La}^{\text{III}}$ ,  $\text{Cu}^{\text{II}}$ , and  $\text{O}^{2-}$  ions converged and the details of the fit are given in Table 1. X-ray data were used to refine the location and occupancy of the two sites for vanadium. Several bond valence sums and coordination environments for the B-cations in the refined structure for this model were chemically unacceptable [14].

The second model is based on an unrotated B-cation plane and at least initially, involves trigonal bipyramidal coordination for the B-cations. To begin, the copper cations were assigned to three of the five B-cation sites, equivalent to the ordering found in the rotated model. The atomic positions converged with decidedly better agreement factors than those of the previous model (see Table 1). The final stage considering over 5100 NPD reflections from the first bank of data ( $90.00^\circ$ ) and 3800 from the second bank ( $144.85^\circ$ ) confirms that there is no rotation of the B-cation plane. The observed, calculated

Table 1

Neutron diffraction data refinement parameters. Parenthetical goodness-of-fit values refer to the second bank of data at 144.85° as opposed to those from the first bank at 90.00°

Formula	La <sub>3</sub> Cu <sub>2</sub> VO <sub>9</sub>	La <sub>3</sub> Cu <sub>2</sub> VO <sub>9</sub>
Space group	<i>P</i> 6 <sub>3</sub> / <i>m</i>	<i>P</i> 6 <sub>3</sub> / <i>m</i>
Model	rotated	unrotated
<i>a</i> (Å)	14.448(1)	14.447(1)
<i>c</i> (Å)	10.686(1)	10.686(1)
<i>V</i> (Å <sup>3</sup> )	965.90(1)	965.73(1)
<i>Z</i>	26/3	26/3
<i>d</i> <sub>calc</sub> (g cm <sup>-3</sup> )	5.502	5.501
<i>R</i> <sub>p</sub> (%)	4.9 (5.4)	4.4 (4.5)
<i>R</i> <sub>wp</sub> (%)	7.6 (8.2)	7.0 (7.0)
$\chi^2$	2.2	1.7
<i>R</i> <sub>f</sub> <sup>2</sup> (%)	9.8 (7.2)	7.6 (6.5)
Reflections	5100 (3800)	5100 (3800)
Coherent scattering lengths	La: 8.24 fm Cu: 7.718 fm V: -0.3824 fm O: 5.805 fm	
Radiation	Neutron Time of Flight (TOF)	
<i>d</i> range (Å)	0.552–4.119	
Software	General Structural Analysis System (GSAS)	
Profile function	Exponential Gaussian convolution (1st TOF profile function in GSAS) (Von Dreele 1978)	
Background correction	Power series: $Q^{2n}/n!$ (4th background function in GSAS)	

and difference NPD patterns for the first bank are plotted in Fig. 5.

Remarkably, the occupancy of one of the copper sites refined to only 0.87(1) while those of the other two refined to 1.00(1). This corresponds to 1.99(1) copper per La<sub>3</sub>Cu<sub>2</sub>VO<sub>9</sub> formula unit. The vanadium positions and occupancies were refined from PXD data. Vanadium was initially assigned to the two crystallographically unique sites (V(1) and V(5)) as well as the remainder of the partially occupied copper site, Cu(2), but the position of the vanadium on this site was not restricted to that of the copper. The refined structural and atomic parameters are listed in Table 2 as well as the bond valence sums for the

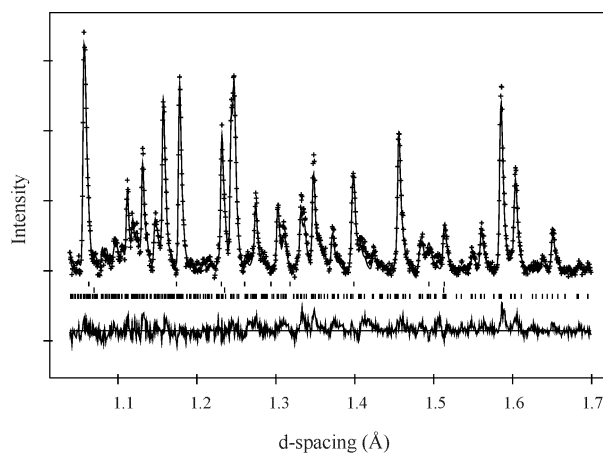


Fig. 5. Observed, calculated and difference neutron powder diffraction data. Extra phases are from the vanadium container and the cadmium shield.

cations [14], which are more sensible than the previous rotated model. Selected bond lengths and angles are given in Tables 3 and 4, respectively.

Despite the cation ordering in the (Cu/V)O<sub>3/3</sub> layer, the positions of the La cations did not change considerably. The hexagonal array of A-cations shows no significant modulations reminiscent of the supercell. The coordination environment of La(1) also remained unchanged with six La–O distances of 2.49(1) Å and two more of 2.67(1) Å. However, the coordination environments of the other two crystallographically independent lanthanum cations did distort slightly. The inner coordination sphere of La(2) still consists of six oxygen, but the bond lengths range from 2.39(1) to 2.68(1) Å. Two more distant oxygen sit 2.77(1) Å away. For La(3), the seven oxygen occupy the inner coordination sphere at distances from 2.33(1) to 2.62(1) Å. One more distant oxygen sits 2.88(1) Å away. The bond valence calculations for the three lanthanum are all close to three and confirm the accuracy of their coordination environments (see Table 2) [14].

The B-cations in the unrotated model exhibit various coordination environments. Fig. 6 shows the B-cation plane for the refined structure with thirteen cation sites per plane, five of which are crystallographically distinct (four *6h* sites and one *2d* site). Six (two *6h* sites) of the thirteen are occupied fully by copper, four (one *6h* and one *2d* site) are occupied fully by vanadium, and three (one *6h*) are shared by copper and vanadium. The coordination environments of the B-cations include trigonal bipyramidal, distorted square planar and distorted

Table 2

Crystallographic data for  $\text{La}_3\text{Cu}_2\text{VO}_9$  based on Rietveld refinement of NPD and PXD data in  $P6_3/m$  with  $a = 14.477(1)$  and  $c = 10.686(1)$  Å. The bond valence sums (BVS) for the cations are listed in the final column and verify the accurateness of the structure

Atom	Site	$x$	$y$	$z$	occupancy	$B_{\text{iso}}$ (Å <sup>2</sup> )	BVS
La(1)	2b	0	0	0	1	0.06(3)	3.1
La(2)	12i	0.3034(1)	0.0732(1)	−0.0005(1)	1	0.45(2)	3.0
La(3)	12i	0.6120(2)	0.1488(1)	0.0085(1)	1	0.30(2)	3.1
V(1)	2d	2/3	1/3	1/4	1	0.64*	4.5
V(2)	6h	0.989(22)	0.134(34)	1/4	0.13(1)	0.81(4)	
Cu(2)	6h	1.0183(3)	0.1562(3)	1/4	0.87(1)	0.81(4)	1.9
Cu(3)	6h	0.3515(2)	0.2284(2)	1/4	1.00(1)	0.51(3)	1.8
Cu(4)	6h	0.6059(3)	0.5807(3)	1/4	1.00(1)	0.92(3)	2.0
V(5)	6h	0.194(4)	0.705(4)	1/4	1	0.64*	5.2
O(a)	12i	0.4378(3)	0.0347(3)	0.0766(2)	1	0.49(3)	
O(b)	12i	0.7471(2)	0.1139(2)	0.0744(3)	1	0.36(4)	
O(c)	12i	0.0485(3)	0.1797(3)	0.0824(2)	1	0.80(4)	
O(d)	4f	2/3	1/3	0.0775(4)	1	0.07(6)	
O(e)	12i	0.2813(3)	0.4982(3)	0.1079(3)	1	0.56(3)	
O(1)	2a	0	0	1/4	1	0.36(7)	
O(2)	6h	0.3103(4)	0.0741(5)	1/4	1	1.03(6)	
O(3)	6h	0.5641(3)	0.3738(3)	1/4	1	0.62(5)	
O(4)	6h	0.2892(6)	0.3474(6)	1/4	1	1.71(7)	
O(5)	6h	0.4528(5)	0.5519(5)	1/4	1	1.39(7)	

\* Thermal parameters for vanadium were set at 0.64 and not refined.

tetrahedral. Only V(1) displays ideal trigonal bipyramidal coordination with  $D_{3h}$  point symmetry. V(5) possesses tetrahedral coordination with the vanadium distorted towards an edge of the tetrahedron. The Cu(2) tetrahedral coordination environment flattens to approximate a square plane. Cu(3) and Cu(4) occupy trigonal bipyramids that distort towards square pyramids. None of these environments are extremely rare for  $\text{Cu}^{\text{II}}$  or  $\text{V}^{\text{V}}$ .

$\text{La}_3\text{Cu}_2\text{VO}_9$  is paramagnetic over the entire range of temperatures measured (5 to 370 K). Since the vanadium is pentavalent,  $\text{Cu}^{\text{II}}$  is the only spin magnetic species. The inverse magnetic susceptibility is shown in Fig. 7, and three distinct paramagnetic regimes can be identified and fit to the Curie–Weiss law,  $\chi_{\text{m}} = C/(T - \theta)$ . The transition between the two low temperature regions is quite narrow ( $\approx 20^\circ$ ) compared to the one between the two high temperature regions which is approximately

$150^\circ$ . Table 5 lists the temperature ranges and the corresponding best-fit parameters for each region.

#### 4. Discussion

PXD and NPD confirm that the structure of  $\text{La}_3\text{Cu}_2\text{VO}_9$  is indeed closely related to that of the rare earth hexagonal phases, and as such it is an  $n = 3$  member of the  $\text{Ln}_n\text{Cu}_{n-1}\text{M}^{n+2}\text{O}_{3n}$  series. The ratio of lanthanum to copper to vanadium in the reaction mixture throughout the synthesis is three to two to one and the refinement verifies that the stoichiometry of the lanthanum and copper did not change.

We have confirmed the hexagonal unit cell reported by Jansson et al. [9] and can further assign a symmetry of  $P6_3/m$ . The atomic structure consists of alternating layers of edge-sharing  $\text{AO}_{6/3}$  octahedra and  $\text{BO}_{3/3}$  planes

Table 3  
Selected bond distances for La<sub>3</sub>Cu<sub>2</sub>VO<sub>9</sub>

Bond	Number	Distance (Å)	Bond	Number	Distance (Å)
La(1)–O(c)	6	2.487(4)	V(1)–O(d)	2	1.843(4)
La(1)–O(c)	2	2.672	V(1)–O(3)	3	1.845(5)
La(2)–O(a)	1	2.4164(5)	Cu(2)–O(c)	2	1.843(2)
La(2)–O(b)	1	2.425(3)	Cu(2)–O(1)	1	2.137(5)
La(2)–O(b)	1	2.555(3)	Cu(2)–O(2)	1	2.159(5)
La(2)–O(c)	1	2.386(5)			
La(2)–O(c)	1	2.482(4)	Cu(3)–O(b)	2	1.879(3)
La(2)–O(e)	1	2.776(4)	Cu(3)–O(2)	1	1.999(8)
La(2)–O(2)	1	2.679(1)	Cu(3)–O(3)	1	2.719(4)
La(2)–O(4)	1	2.774(2)	Cu(3)–O(4)	1	2.305(11)
La(3)–O(a)	1	2.331(4)	Cu(4)–O(a)	2	1.867(3)
La(3)–O(a)	1	2.543(5)	Cu(4)–O(2)	1	2.023(8)
La(3)–O(b)	1	2.362(5)	Cu(4)–O(3)	1	2.738(6)
La(3)–O(d)	1	2.484(3)	Cu(4)–O(5)	1	2.036(9)
La(3)–O(e)	1	2.567(5)			
La(3)–O(e)	1	2.615(6)	V(5)–O(e)	2	1.546(9)
La(3)–O(3)	1	2.634(2)	V(5)–O(4)	1	2.005(66)
La(3)–O(5)	1	2.877(3)	V(5)–O(5)	1	1.988(47)
Cu(4)–Cu(5)	3	3.35(1)	Cu(4)–Cu(4)	3	3.70(1)
Cu(5)–Cu(6)	3	3.53(1)	Cu(5)–Cu(5)	3	7.73(1)
Cu(6)–Cu(4)	3	3.79(1)	Cu(6)–Cu(6)	3	10.19(1)

similar to YAlO<sub>3</sub>. It is clear from the refinement that the B-cations order within the plane to create a supercell which is thirteen times larger than a fundamental cell common to the rare earth hexagonal phases ( $a \approx 4 \text{ \AA}$ ,  $c \approx 11 \text{ \AA}$ ). In contrast to a model based on a rotated B-cation plane, this model yields reasonable bond distances and coordination environments for all the cations, and decidedly leads to the best fit with experimental data.

Given their respective oxidation states, it is not unexpected to find Cu<sup>II</sup> and V<sup>V</sup> in ordered sites, but this could be accomplished with perfect ordering in a supercell that is only three times larger. In the latter case, the B-cations would likely all experience trigonal bipyramidal coordination and no small triangles of copper cations would occur. Apparently, the clustering of B-cations in a larger unit cell is preferable

over a more uniform distribution. The particular B-cation arrangement in the thirteen times larger supercell also affords a more suitable set of B-cation coordination environments with some of the vanadium and copper occupying distorted tetrahedral sites. Overall it appears that Cu<sup>II</sup>/V<sup>V</sup> in a 2/1 ratio is best accommodated by a supercell which creates  $3 + 3 + 3 + 3 + 1 = 13$  B-cation coordination environments per plane, ten of which are distorted from  $D_{3h}$  symmetry.

The inverse susceptibility of La<sub>4</sub>Cu<sub>3</sub>MoO<sub>12</sub> exhibited two paramagnetic regimes. The copper cations form triangular clusters with an intermetallic distance of approximately 3.4 Å. These behave as either 1 or 3 independent 1/2 spins, and indeed the magnetic regimes clearly correspond to 1 and 3 paramagnetic spins per formula unit [6]. This is expected for triangular clusters in which two spins

Table 4  
Selected bond angles for  $\text{La}_3\text{Cu}_2\text{VO}_9$

Bonds	Angle ( $^\circ$ )
O(d)–V(1)–O(d)	180.0(2)
O(d)–V(1)–O(3)	90.0
O(3)–V(1)–O(3)	120.0
O(c)–Cu(2)–O(c)	155.0(3)
O(c)–Cu(2)–O(1)	95.0(2)
O(c)–Cu(2)–O(2)	93.1(2)
O(1)–Cu(2)–O(2)	141.5(3)
O(b)–Cu(3)–O(b)	161.0(2)
O(b)–Cu(3)–O(2)	98.7(2)
O(b)–Cu(3)–O(3)	82.7(2)
O(b)–Cu(3)–O(4)	85.0(2)
O(2)–Cu(3)–O(3)	116.9(3)
O(2)–Cu(3)–O(4)	145.3(3)
O(3)–Cu(3)–O(4)	98.7(2)
O(a)–Cu(4)–O(a)	165.8(3)
O(a)–Cu(4)–O(2)	94.7(2)
O(a)–Cu(4)–O(3)	83.2(2)
O(a)–Cu(4)–O(5)	88.9(2)
O(2)–Cu(4)–O(3)	113.4(3)
O(2)–Cu(4)–O(5)	147.8(4)
O(3)–Cu(4)–O(5)	98.8(2)
O(e)–V(5)–O(e)	158.5(34)
O(e)–V(5)–O(4)	98.4(25)
O(e)–V(5)–O(5)	97.3(19)
O(4)–V(5)–O(5)	85.4(18)

can order antiferromagnetically and the third then can not. The single spins on the triangular clusters interact weakly owing to the long inter-cluster distance (7.9 Å) and order antiferromagnetically at 5 K.

The magnetism of  $\text{La}_3\text{Cu}_2\text{VO}_9$  is also completely paramagnetic at high temperature. By 330 K, the slope of the high temperature region (III) is quite close to the expected value for 1/2 spins (expected  $p_{\text{eff}} = 1.73$ ). The large negative Weiss temperature for this regime (–470 K) denotes the strong antiferromagnetic coupling. Despite this forceful interaction, the spins do not order completely below 200 K. This is because of the geometric frustration that results from triangular spin arrange-

ments. The slopes of regions II and I correspond to less paramagnetic spin, and the Weiss temperatures (–94 K and –6.6 K, respectively) indicate that the spin interactions are much weaker.

The copper cations in the B-cation plane of  $\text{La}_3\text{Cu}_2\text{VO}_9$  form nine-atom clusters (see Fig. 6) similar to  $\text{Cu}_9\text{X}_2(\text{cpa})_6$ , X = F, Cl, Br, which also exhibits three regions in  $1/\chi_m$  plots [15]. A cluster consists of a triangle of triangular clusters which each have an intermetallic distance of approximately 3.6 Å. If each triangle can theoretically behave as 1 or 3 independent 1/2 spins, we might expect a triangle of triangles to yield spin regimes that correspond to 1, 3 and 9 paramagnetic spins. However, there are many other ways to associate the copper into triangular clusters as Fig. 6 suggests. For example, there is a fourth triangular cluster centered on O(1) with an intermetallic distance of 3.7 Å.

The structural refinement indicates that the average number of copper cations per cluster is 8.67. Given that one site is only 87% occupied by  $\text{Cu}^{\text{II}}$ , the microscopic cluster population is 66% 9-copper clusters, 30% 8-copper clusters and 4% 7-copper clusters. Assuming that at 370 K the sample is 100% paramagnetic, the bulk susceptibility measurements show that the clusters exhibit average spin states of 0.96, 4.00 and 8.67 paramagnetic spins in the different temperature ranges. The ratio of the susceptibility of the first and third temperature regimes is 9.0, which agrees moderately well with the average number of coppers per cluster. The susceptibility of the second regime of 4.00 cannot be easily interpreted with regard to a 9-copper cluster since it is impossible to pair up five spins and leave four unpaired. The presence of 8- and 7-copper clusters should decrease the overall paramagnetic fraction by alleviating spin frustration, but only by as much as an average of 0.38 spins per cluster. Given the complex geometry of the cluster, quantum mechanical calculations will likely be required to model the spin system. Field dependent measurements could also help to quantify the magnetic transitions as in the molybdate case [7].

Previous electron diffraction studies were used to support an even larger monoclinic supercell of  $a_m = 14.4427$ ,  $b_m = c_h = 10.685$ ,  $c_m = 52.07$  Å,  $\beta = 106.1^\circ$ , and  $Z_m = 4Z_h$ , which corresponds to one possible tiling of the monoclinic  $ac$  plane equivalent in area to four hexagonal basal units [9]. Higher order Laüé zone ring radii,  $r$ , from CBED patterns for different crystal orientations can be used to determine real lattice spacings,  $H_m^{-1}$  [16]. Fig. 3 shows three such rings for the  $[1\bar{1}00]$  direction. Calculated values are based on the

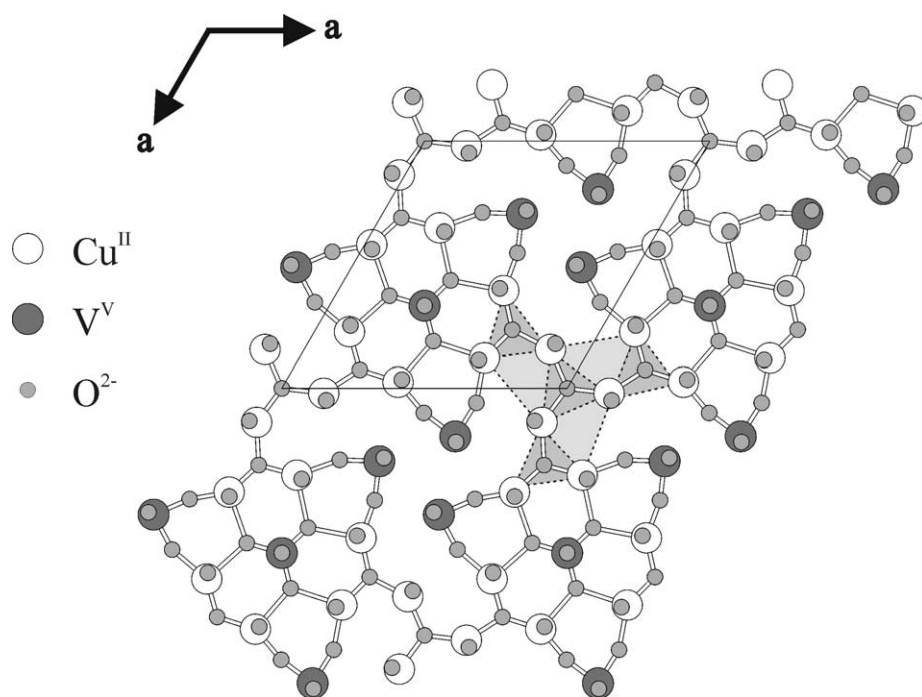


Fig. 6. (Cu/V)O<sub>3</sub> plane for La<sub>3</sub>Cu<sub>2</sub>VO<sub>9</sub>. Triangle of triangular copper clusters is centered on O(1).

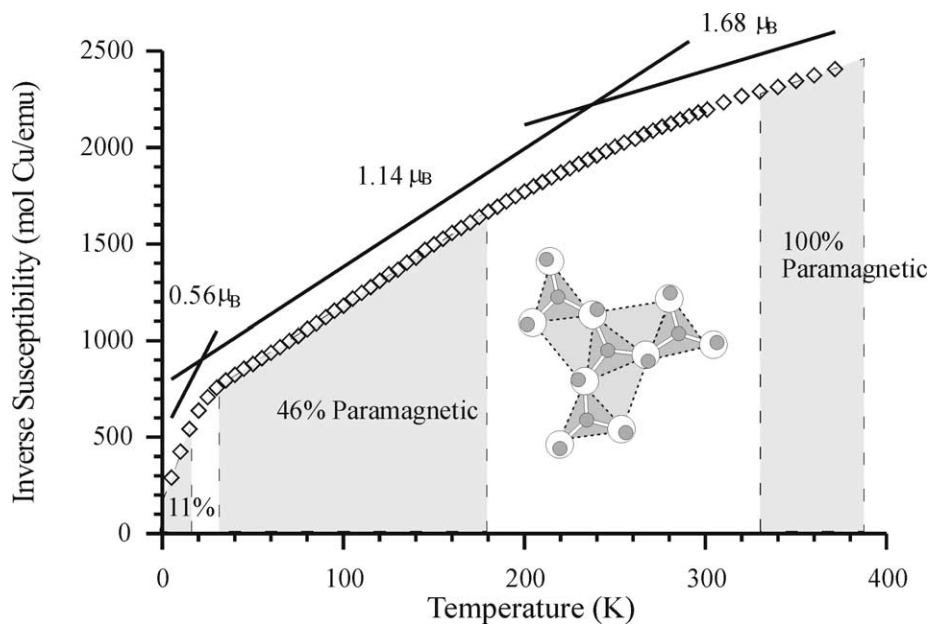


Fig. 7. Inverse susceptibility for La<sub>3</sub>Cu<sub>2</sub>VO<sub>9</sub> per mole of Cu<sup>II</sup>. Three paramagnetic regimes of distinct slope are shaded which correspond closely to 1/9, 4/9 and 9/9 spins per copper.

Table 5  
Magnetic data for  $\text{La}_3\text{Cu}_2\text{VO}_9$

Region	Temperature range (K)	$\theta$ (K)	$C$ ( $\text{emu K mol}^{-1}$ of Cu)	$p_{\text{eff}}$ ( $\mu_B$ )	Relative spin fraction
I	5–15	–6.6	0.040	0.56	1.00
II	35–180	–94	0.16	1.14	4.15
III	330–370	–470	0.35	1.68	9.00

Table 6  
Calculated and measured layer spacings ( $H^{-1}$ ) from convergent beam electron diffraction

Crystal orientation	Laüé zone order	Calculated $H^{-1}$ (nm)	Measured $H^{-1}$ (nm)
$2\bar{1}0$	1st	3.81	3.80
112	1st	2.58	2.58
114	1st	4.51	4.59
$3\bar{1}0$	1st	5.19	5.15
$1\bar{1}0$	1st	2.49	2.49
$1\bar{1}0$	2nd	1.45	1.23
$1\bar{1}0$	3rd	0.83	0.82

chosen unit cell. The ratio between the measured and calculated values should correspond to the order of the Laüé zone. Excellent agreement between the measured values and calculations based on the hexagonal supercell which is thirteen times larger imply that an even larger supercell is unnecessary. Table 6 lists the measured and calculated  $H^{-1}$  values.

$\text{Ln}_3\text{Cu}_2\text{VO}_9$ ; Ln = Pr, Nd, Eu–Gd, samples have been made in a similar fashion to that of the lanthanum analogue, and gadolinium appears to be the limit of the analogues that have a comparable powder diffraction pattern. Fig. 8 shows the lattice parameters for  $\text{Ln}_{3-x}\text{La}_x\text{Cu}_2\text{VO}_9$ ;  $x = 0, 1.0, 2.0, 2.5, 3.0$ ; Ln = Pr, Nd, Sm, Eu, and Gd. The  $a$  parameters of all the samples behave linearly as expected, similar to the molybdate family. The  $c$  parameters, however, do not change monotonically. The heights of the unit cells for solid solution compositions do not change significantly as a smaller lanthanide is partially substituted ( $x = 1.0$  and  $2.0$ ) for the lanthanum. Only the end-members exhibit notably different  $c$  parameters. This aberration likely results from the superstructure. The irregular set of B-cation coordination environments disrupts the regular interpolyhedral connections between the  $\text{AO}_{6/3}$  and  $\text{BO}_{3/3}$  layers.

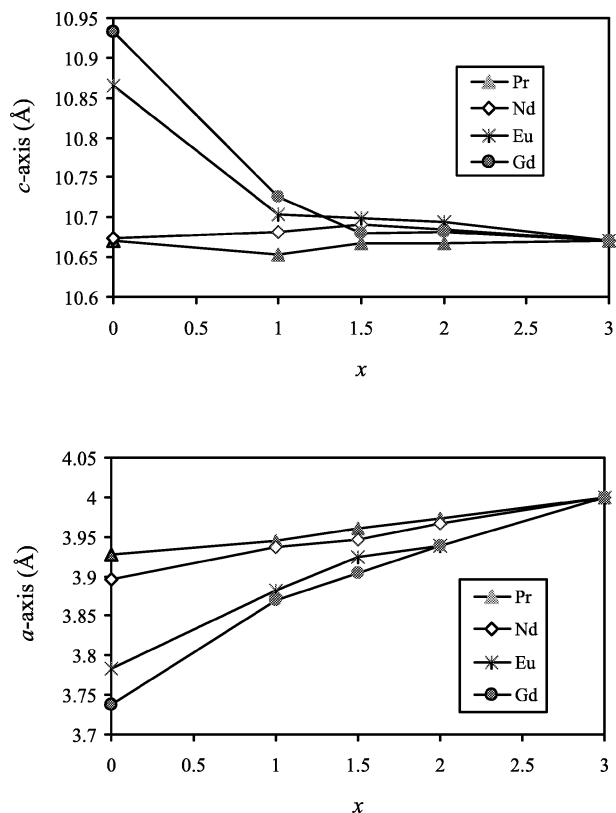


Fig. 8. Graph of lattice parameters for  $\text{Ln}_{3-x}\text{La}_x\text{Cu}_2\text{VO}_9$  as a function of  $x$ .

This can be seen by comparing the positions of the oxygen between the A- and B-cations for the molybdenum and vanadium analogues. The deviation in the  $z$  coordinates for the oxygen around the A-cation is  $0.4 \text{ \AA}$  for  $\text{La}_3\text{Cu}_2\text{VO}_9$  but only  $0.1 \text{ \AA}$  for  $\text{La}_4\text{Cu}_3\text{MoO}_{12}$ . Consequently, the interaction between the layers is more discontinuous for the vanadate as the A-cation array contracts.

The rare earth hexagonal structure, while seemingly unsatisfactory for many  $\text{ABO}_3$  compositions, has proven to be a versatile type for accommodating cations in less

common coordination environments. The possibilities are especially sensitive to the small B-cations. No perturbation is necessary if they prefer trigonal bipyramidal coordination. However, cation ordering phenomena can lead to novel sets of B-cation coordination environments which can accommodate various potential B-cation stoichiometries.

$\text{La}_3\text{Cu}_2\text{VO}_9$  is an  $(\text{ABO}_3)_n=3$  phase that facilitates a B-cation composition of two-thirds  $\text{Cu}^{\text{II}}$  and one-third  $\text{V}^{\text{V}}$ . This heretofore unknown superstructural variation of the rare-earth hexagonal structure type is a function of the transition metal coordination preferences. Other compositions could well lead to other superstructures. Solid solutions between the  $n = 2, 3$  and 4 members of the  $\text{Ln}_n\text{Cu}_{n-1}\text{M}^{n+2}\text{O}_{3n}$  series would make it possible to achieve any Cu/M ratio between one and three. The ratio of the transition metal cations in  $\text{La}_{13}\text{Cu}_9\text{V}_3\text{MoO}_{39}$  could occupy thirteen sites of the hexagonal supercell without disorder. Other compositions may promote different cation ordering schemes and different superstructures. Frustrated magnetism would likely result if the spin lattices are partially occupied hexagonal arrays and must result if the Cu/M ratio is greater than two.

It is notable that the more copper on the B-site, the wider the range of tolerable A-cation sizes.  $\text{Ln}_3\text{Cu}_2\text{VO}_9$  accommodates  $\text{Ln} = \text{La}, \text{Pr}, \text{Nd}, \text{Eu},$  and  $\text{Gd}$ ; and  $\text{Ln}_4\text{Cu}_3\text{MoO}_{12}$  accommodates  $\text{Ln} = \text{La}, \text{Pr}, \text{Nd}, \text{Sm}-\text{Tm}$  [17]. Both families form with lanthanum where previously europium was the largest known trivalent cation ever incorporated in the rare-earth hexagonal structure type. This points to the ability of copper along with large lanthanides to promote the formation of the rare-earth hexagonal structure by destabilizing multiphase alternatives. Solid state compounds exist in a delicate balance of interatomic forces often far to complex to anticipate.  $\text{La}_3\text{Cu}_2\text{VO}_9$  and the other members of the rare-earth hexagonal cuprates testify to the intimate role of copper in the structural counterpoise.

## Acknowledgements

This work is supported by a National Science Foundation (NSF) graduate fellowship for DAVG, and made use

of the Central Facilities at the Materials Research Center of Northwestern University (NSF DMR-9632472). S.J.B. and N.M.D. participated in the 1999 MASEC Summer Research Program for undergraduates at the Materials Research Center Northwestern University (NSF DMR-9632472). We would like to thank Dr. James Jorgensen and Dr. Simine Short for carrying out the neutron diffraction experiment. The IPNS is supported by the Department of Energy (W-31-109-ENG-38).

## References

- [1] D.M. Giaquinta, H.-C. zur Loye, *Chem. Mater.* 6 (1994) 365.
- [2] D.M. Adams, *Inorganic Solids*, Vol. 5, Wiley, London, 1974, p. 105.
- [3] E.F. Bertaut, J. Mareschal, *Comptes Rendus* 275 (1963) 867.
- [4] S.J. Schneider, *J. Res. NBS* 65A (1961) 429.
- [5] D.A. Vander Griend, S. Boudin, K.R. Poeppelmeier, M. Azuma, H. Toganoh, M. Takano, *J. Am. Chem. Soc.* 120 (1998) 11518.
- [6] D.A. Vander Griend, S. Boudin, V. Caignaert, K.R. Poeppelmeier, Y. Wang, V.P. Dravid, M. Azuma, M. Takano, Z. Hu, J. Jorgensen, *J. Am. Chem. Soc.* 121 (1999) 4787.
- [7] M. Azuma, T. Odaka, M. Takano, D.A. Vander Griend, K.R. Poeppelmeier, Y. Narumi, K. Kindo, Y. Mizuno, S. Maekawa, *Phys. Rev. B* 62 (2000) 3588.
- [8] M.T. Anderson, K.B. Greenwood, G.A. Taylor, K.R. Poeppelmeier, *Progr. Solid State Chem.* 22 (1993) 197.
- [9] K. Jansson, I. Brynste, Y. Teraoka, *Mater. Res. Bull.* 31 (1996) 827–835.
- [10] A.J.C. Wilson, *International Tables for Crystallography*, Vol. C, Kluwer Academic Publishers, Dordrecht/Boston/London, 1995.
- [11] A. Larson, R.B. Von Dreele, *The General Analysis System*, Los Alamos National Laboratory, Los Alamos, NM, 1985.
- [12] O. Terasaki, J.M. Thomas, S. Ramdas, *J. Chem. Soc. Chem. Commun.* (1984) 216.
- [13] O. Terasaki, J.M. Thomas, G.R. Millward, *Proc. Roy. Soc. London Ser. A* 395 (1984) 153.
- [14] I.D. Brown, D. Alternatt, *Acta Cryst. Sect. B* 41 (1985) 244.
- [15] S. Maruti, L.W. ter Haar, *J. Appl. Phys.* 75 (1994) 5949.
- [16] M. Raghavan, J.C. Scanlon, J.W. Steeds, *Met. Tran.* 15A (1984) 1299.
- [17] D.A. Vander Griend, S. Malo, T.K. Wang, K.R. Poeppelmeier, *J. Am. Chem. Soc.* 122 (2000) 7308.